Wafer-Level Photocatalytic Water Splitting on GaN Nanowire Arrays Grown by Molecular Beam Epitaxy

Defa Wang,[†] Adrien Pierre,[†] Md Golam Kibria,[†] Kai Cui,[†] Xueguang Han,[†] Kirk H. Bevan,[‡,§] Hong Guo,[∥] Suzanne Paradis,[⊥] Abou-Rachid Hakima,[⊥] and Zetian Mi*[,†]

[†]Department of Electrical and Computer Engineering, McGill University, 3480 University Street, Montreal, Quebec H3A 2A7, Canada

[‡]Department of Mining and Materials Engineering, McGill University, 3600 University Street, Montreal, Quebec H3A 2T8, Canada

[§]Materials Science and Technology Division, Oak Ridge National Laboratory, Oak Ridge, Tennessee 37831, United States

[∥]Centre for the Physics of Materials, Department of Physics, McGill University, 3610 University Street, Montreal, Quebec H3A 2T8, Canada

[⊥]Defence Research and Development Canada Valcartier, 2459 Boulevard Pie XI North, Quebec, Quebec G3J 1X5, Canada

Supporting Information

ABSTRACT: We report on the achievement of wafer-level photocatalytic overall water splitting on GaN nanowires grown by molecular beam epitaxy with the incorporation of Rh/Cr_2O_3 core−shell nanostructures acting as cocatalysts, through which H_2 evolution is promoted by the noble metal core (Rh) while the water forming back reaction over Rh is effectively prevented by the Cr_2O_3 shell O_2 diffusion barrier. The decomposition of pure water into H_2 and O_2 by GaN nanowires is confirmed to be a highly stable photocatalytic process, with the turnover number per unit time well exceeding the value of any previously reported GaN powder samples.

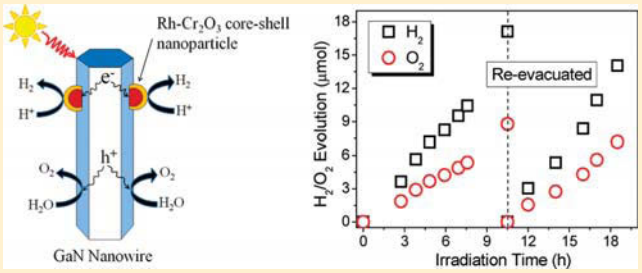

KEYWORDS: GaN, nanowire, water splitting, hydrogen, photocatalytic, molecular beam epitaxy

Since the discovery of the Honda−Fujishima effect in a TiO_2/Pt photoelectrochemical cell in the early 1970s,[1−3] the use of semiconductors for photocatalytic water splitting has attracted tremendous interest: for it enables the generation of clean and renewable hydrogen fuel directly from solar irradiation without the consumption of electric power. Semiconductor photocatalytic water splitting generally involves three fundamental processes: (i) band gap absorption of photons and excitation of electron−hole pairs; (ii) separation and migration of photogenerated charge carriers; (iii) surface redox reactions via photogenerated electrons and holes. Thermodynamically, if the conduction band minimum is more negative than the reduction potential of H^+/H_2 (0 V vs normal hydrogen electrode (NHE)) and the valence band maximum is more positive than the oxidation potential of O_2/H_2O (1.23 V vs NHE), then water molecules can be reduced by electrons to form H_2 and oxidized by holes to form O_2 to achieve overall water splitting. Over the past 4 decades, the development of photocatalysis has primarily focused upon large band gap metal oxides involving ions with filled or empty d-shell bonding configurations (i.e., Ti^{4+}, Zr^{4+}, Nb^{5+}, Ta^{5+}, W^{6+}, Ga^{3+}, In^{3+}, Ge^{4+}, Sn^{4+}, and Sb^{5+})[4−6] and oxynitrides such as $(Ga_{1-x}Zn_x)(N_{1-y}O_y)$.[2,7] Recently, the use of group III nitride semiconductors for water splitting has attracted considerable attention.[8,9] Due to the more negative potential of the nitrogen 2p orbital, compared to that of the oxygen 2p orbital, metal nitrides often possess a narrow band gap and can potentially encompass nearly the entire solar spectrum. Moreover, the inherent chemical stability of nitrides also favors their use in the harsh photocatalysis reaction environment.[10] Indeed, recent first-principles calculations suggest that a single H_2O molecule can be efficiently cleaved in an *exothermic* reaction to form H_2 under photoexcitation at Ga-terminated surface sites.[11] Ab initio molecular dynamic simulations further show that the overall water oxidation reaction at GaN surfaces can be energetically driven by photogenerated holes.[12]

The size, morphology, surface chemistry, and crystal structure of photocatalysts often play a crucial role in determining their photophysical and photocatalytic properties. Conventional photocatalysts are typically employed in the form of powders. However, photocatalysts in the form of one-dimensional (1-D) nanostructures, such as nanowires, nanobelts, and nanotubes, are highly desired.[13−20] These nanomaterials exhibit extremely large

Received: February 28, 2011
Revised: April 24, 2011
Published: May 13, 2011

dx.doi.org/10.1021/nl2006802 | *Nano Lett.* 2011, 11, 2353–2357

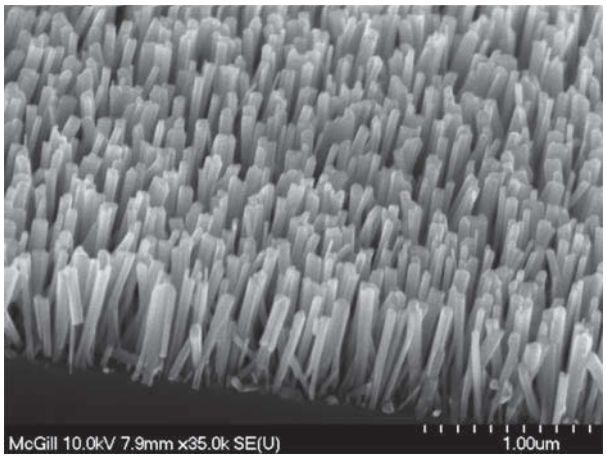

Figure 1. A 45°-tilted SEM image showing the morphology of GaN nanowires grown on a Si(111) substrate by molecular beam epitaxy.

surface-to-volume ratios and significantly enhanced light absorption. More importantly, ballistic charge transport along single-crystal nanowires is much more efficient than the diffusive transport in powdered materials. Additionally, 1-D nanostructures allow control over the photocatalyst crystal plane promoting either H_2 or O_2 evolution.[16] Consequently, significantly enhanced photocatalytic activity is expected from 1-D nanoscale materials. In this work, we have investigated, for the first time, the use of GaN nanowire arrays for pure water splitting, wherein the reaction primarily occurs on the Ga-face nonpolar lateral surfaces (*m*-plane). The capacity of GaN nanowires for water splitting is unambiguously confirmed by utilizing the hole-scavenger CH_3OH and the electron-acceptor $AgNO_3$ to respectively fuel H_2 and O_2 half-reactions. To further enable highly efficient water splitting, we have incorporated cocatalytic Rh/Cr_2O_3 core−shell nanostructures on the lateral GaN nanowire surfaces and have observed, for the first time, photocatalytic *overall* water splitting on metal nitride nanowires. We have demonstrated that the decomposition of pure water into H_2 and O_2 by GaN nanowires is a highly stable photocatalytic process, with the amount of H_2 and O_2 generated well exceeding that of the host GaN nanowire photocatalytic material in a few hours. The resulting turnover number is much higher than previously reported values achieved on GaN powder samples.[21]

The catalyst-free GaN nanowires were grown on a Si(111) substrate using a radio frequency plasma-assisted molecular beam epitaxial (MBE) system under nitrogen-rich conditions.[22] Growth conditions include the following: a temperature of ∼750 °C, nitrogen flow rate of 1−2 sccm, and a forward plasma power of ∼400 W. Shown in Figure 1 is a typical 45°-tilted scanning electron microscopy (SEM) image of the GaN nanowires. The wires possess a wurtzite crystal structure and are vertically aligned to the substrate, with the growth direction along the *c*-axis. The areal density of the nanowires is estimated to be ∼1 × 10^{10} cm^{-2}. The wires exhibit a high degree of size uniformity; their densities, diameters, and lengths can be controlled by varying the growth conditions. We have also confirmed that the GaN nanowire lateral surfaces are Ga-face by etching in a KOH solution.[23] Compared to previously reported powder samples, epitaxial GaN nanowires exhibit superior structural, electrical, and optical properties, which (in conjunction with their extreme chemical stability and large specific surface area) promise

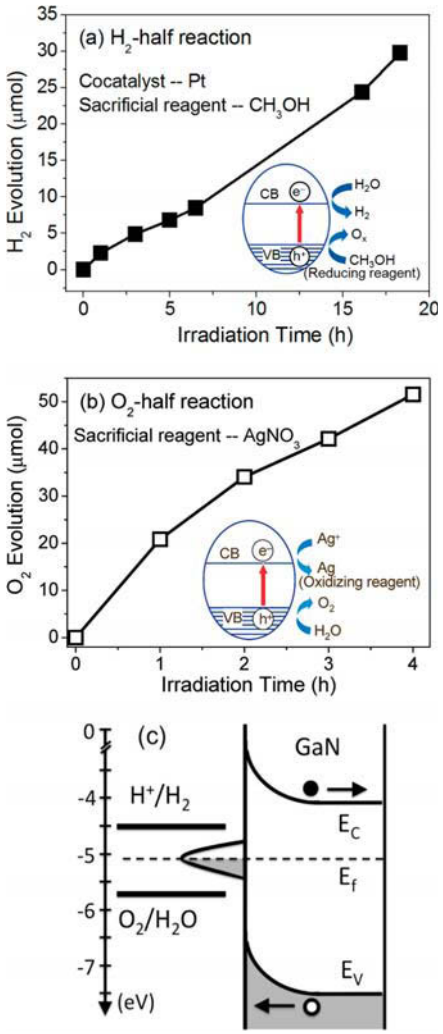

Figure 2. (a) H_2 and (b) O_2 evolution half-reactions in the presence of respective sacrificial reagents over GaN nanowires under a 300 W full arc xenon lamp irradiation. The corresponding reaction processes are schematically illustrated in the insets. (c) GaN surface defects pin the Fermi level at the surface and bend the bands upward, thereby driving holes to the nanowire sidewall and electrons into the bulk.

significantly enhanced photocatalytic activity. In the subsequent experiments, GaN nanowire samples with areas of ∼4 cm^2 are utilized—corresponding to ∼5 μmol of GaN material volume.

The photocatalytic reactions were performed by adopting a 300 W xenon lamp as an outer irradiation source and a reaction chamber with a quartz lid that secures adequate transmittance of UV and visible light. A gas chromatograph (GC-8A, Shimadzu) equipped with a thermal conductivity detector (TCD) was employed for the evaluation of evolved gases (H_2 and/or O_2). We begin our investigation of photocatalytic activity on GaN nanowire surfaces (i.e., the lateral nonpolar *m*-plane, Ga-terminated surfaces) by independently studying the H_2 and O_2 half-reactions in the presence of respective sacrificial reagents. When a photocatalytic reaction is carried out in an aqueous solution consisting of a reducing reagent (i.e., an electron donor or hole scavenger such as alcohol), photogenerated holes irreversibly oxidize the reducing reagent instead of water and thereby enhance H_2 evolution. On the other hand, when photogenerated

dx.doi.org/10.1021/nl2006802 |*Nano Lett.* 2011, 11, 2353–2357

electrons in the conduction band are consumed by oxidizing reagents (i.e., electron acceptors or electron scavengers such as Ag^+ and Fe^{3+}), O_2 evolution reaction is enhanced. For the GaN nanowires, we have used CH_3OH as a hole scavenger to conduct the H_2 half-reaction and $AgNO_3$ as an electron acceptor to perform the O_2 half-reaction, respectively. The evolution of H_2 and O_2 over time is shown in panels a and b of Figure 2, respectively—the corresponding reaction processes are schematically illustrated in the insets. More than 5 μmol of H_2 and 50 μmol of O_2 are produced after 4 h, which demonstrates that GaN nanowires satisfy the photocatalysis thermodynamic and kinetic potentials for H_2 and O_2 evolution.[24] Moreover, we have compared these results with those of GaN powders and planar GaN surfaces: the results demonstrate that the photocatalytic activity of our nanowire samples is remarkably higher than either powder or planar samples under the same experimental conditions (see Figures S4 and S5 in Supporting Information). These observations are consistent with recent theoretical studies. The energy barriers for the first and second H-atom splitting on a pristine Ga-face are predicted to be ~0.10 and 1.42 eV, respectively, which can be easily satisfied by the energy band potentials of GaN (E_g = 3.4 eV, see Figure S1 in Supporting Information) upon band gap excitation.[11] Additionally, ab initio molecular dynamic simulations further show that the overall water oxidation reaction at GaN nonpolar surfaces involves four proton-coupled electron transfer intermediate steps and can be energetically driven by photogenerated holes.[12] The significantly reduced photocatalytic activity of GaN powder samples, on the other hand, may be directly related to the uncontrolled surface polarity.[11] As shown by recent first-principles calculations, the cleavage of water molecules to generate H_2 gas has been predicted to be a much more active process on Ga-terminated surface sites compared to N-terminated surface sites—due to the much smaller absorption energies of H_2 molecules on the Ga-terminated surface sites.[11] This picture is consistent with earlier theoretical predictions,[24] which demonstrate that the unoccupied surface states driving electron transfer to H^+ are localized on Ga-terminated surface sites.

Though H_2 generation on the Ga-face is expected to be exothermic and therefore very efficient under idealized theoretical conditions, in practice, semiconductor photocatalysis reaction rates are strongly influenced by surface charge properties.[25] Due to the presence of dangling bonds and/or surface defects, Fermi-level pinning is commonly observed on GaN surfaces,[26,27] which may significantly degrade the photocatalytic activity through enhanced nonradiative recombination. Such defects also reduce the number of pristine sites available for H_2 evolution. Furthermore, due to the dominant n-type character of GaN, surface defects tend to pin GaN bands upward[25] (as shown in Figure 2c), resulting in a built in electric field which both (1) drives excited electrons away from surface reaction sites and (2) provides an electron tunneling barrier, thereby exponentially reducing the rate of electron transfer to H^+ ions.[25−27] For these reasons, as well as the experimental demonstration that O_2 generation is a much more efficient process than H_2 generation as shown in panels a and b of Figure 2, it is essential to incorporate a suitable cocatalyst that can provide reaction sites and enable efficient electron transfer to the surface by unpinning the bands at the cocatalyst/GaN interface. Such a practice has been employed with most semiconductor photocatalysts developed to date in order to achieve efficient pure water splitting.[28−31]

Noble metals such as Pt and Rh are excellent promoters of H_2 evolution but can also catalyze a backward reaction to form water (H_2O) from H_2 and O_2, thereby limiting their usefulness as cocatalysts for overall photocatalytic water splitting. To avoid the H_2O forming back reaction, a transition-metal oxide that does not catalyze H_2O formation from H_2 and O_2 is usually employed as a diffusion barrier coating to prevent O_2 interaction with the noble metal surface. Among the cocatalysts developed to date, core−shell-structured noble-metal/Cr_2O_3 nanoparticles dispersed on a photocatalyst have been proven to enable H_2 formation in oxynitride solid solutions.[31] The deposition of such cocatalysts on nanowire surfaces may be achieved through impregnation, adsorption, or photodeposition. Among these methods, photodeposition is easily applied to almost all noble metals. Most importantly, the cocatalyst nanoparticles can be selectively deposited on the active sites of the photocatalyst surface, since the metal cations in aqueous solution are reduced by photogenerated electrons into metal nanoparticles—which are always deposited on the surface of photocatalyst where electrons reside. In this regard, we have investigated the photodeposition of Rh/Cr_2O_3 core−shell nanoscale cocatalysts on our GaN nanowires. Importantly, Rh forms a Schottky contact with GaN, thereby overcoming the exposed GaN surface band pinning which is detrimental to the efficient transfer of electrons to H^+ ions in photoelectrolysis.[25] Details on the photodeposition process can be found in the Supporting Information.

Scanning transmission electron microscopy (STEM, FEI Titan 80-300 Cubed equipped with an aberration corrector of the probe-forming lens and a high brightness electron source) was used to characterize the Rh/Cr_2O_3 core−shell nanostructures photodeposited on the GaN nanowires. Illustrated in Figure 3a, a fairly uniform distribution of Rh/Cr_2O_3 nanoparticles on the GaN nanowire lateral surfaces can be clearly seen. Panels b and c of Figure 3 show a typical high-resolution transmission electron microscopy (HRTEM) image and a high-resolution high-angle annular dark field (HR-HAADF) image of the Rh/Cr_2O_3 core−shell nanostructures photodeposited on the GaN nanowires. We can see that each GaN nanowire exhibits the nature of a single crystalline structure. For the Rh/Cr_2O_3 core−shell structure, the metallic Rh core is well crystallized while the Cr_2O_3 shell is likely amorphous. Moreover, electron energy loss spectrometry spectrum image (EELS-SI) was performed to study the elemental distribution in the Rh/Cr_2O_3 core−shell nanostructure. In Figure 4 the HR-HAADF and EELS images, corresponding individual element maps, and RGB images further show clearly the Rh/Cr_2O_3 core−shell nanostructure deposited on GaN nanowires. By combining the HRTEM/HAADF images and the element mapping images, we have clearly confirmed that the Rh/Cr_2O_3 core−shell nanostructures were successfully photodeposited on the lateral surfaces of the GaN nanowires.

Subsequently, overall photocatalytic water splitting was carried out using the GaN nanowires photodeposited with Rh/Cr_2O_3 core−shell nanostructures in pure water, wherein the H_2 evolution was promoted by the noble metal (Rh) core while the backward reaction over the noble metal (water formation from H_2 and O_2) was prevented by the Cr_2O_3 shell.[32] In fact, this has also been verified by our own control experiment: without depositing a Cr_2O_3 oxide shell to cover the Rh nanoparticle core, pure water splitting was not observed because noble metals, such as Rh and Pt, usually act to promote the $H_2 + O_2 \rightarrow H_2O$ back reaction. A visual scheme of the pure water splitting process by GaN nanowires is illustrated in Figure 5a. As expected, overall water splitting has been realized successfully on the GaN

dx.doi.org/10.1021/nl2006802 |*Nano Lett.* 2011, 11, 2353–2357

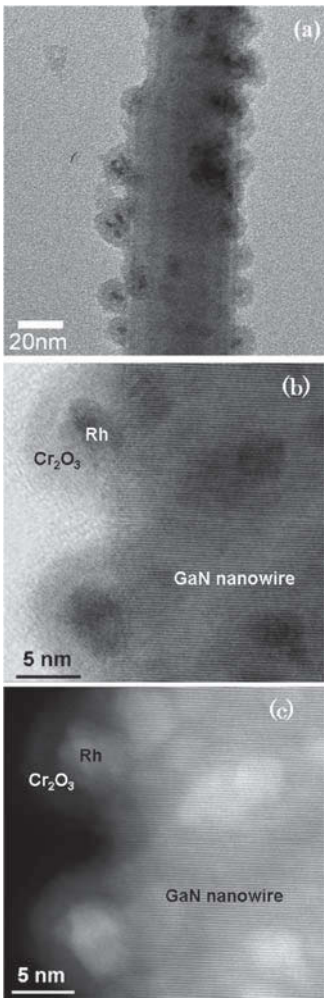

Figure 3. (a) Low magnification TEM image shows uniform distribution of the Rh/Cr_2O_3 nanoparticles on GaN nanowire surfaces. (b) HRTEM image and (c) HR-HAADF image clearly show the Rh/Cr_2O_3 core−shell nanostructures deposited on GaN nanowires.

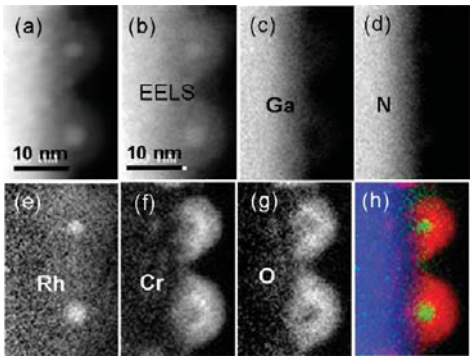

Figure 4. (a) HR-HAADF image and (b) EELS mapping image, (c−g) corresponding individual element mapping images, and (h) RGB image (red, Cr; green, Rh; blue, Ga), clearly showing the Rh/Cr_2O_3 core−shell nanostructure deposited on GaN nanowires.

nanowires photodeposited with Rh/Cr_2O_3 core−shell nanostructures. Figure 5b shows the typical evolution of the photocatalytic water splitting reaction over time. In the two cycles

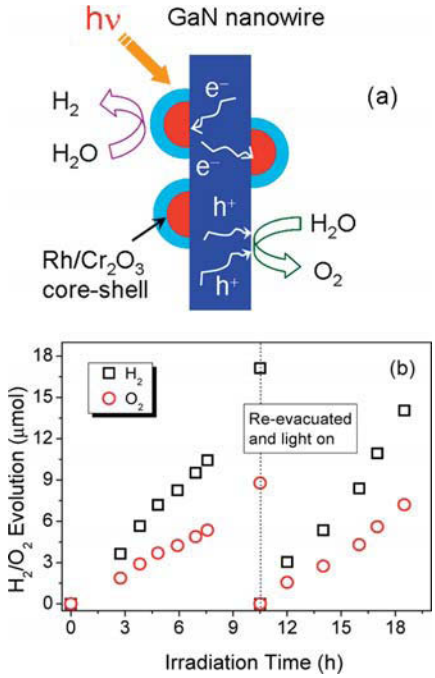

Figure 5. (a) Schematic illustration of water splitting on GaN nanowires with the incorporation of Rh/Cr_2O_3 core−shell nanostructures as cocatalysts. (b) Experimental overall photocatalytic water splitting on Rh/Cr_2O_3 core−shell nanostructure deposited GaN nanowires, under a 300 W full arc xenon lamp irradiation for a duration of 18 h. No degradation of the photocatalytic activity was observed during the course of two cycles of reaction.

displayed in Figure 5 totaling ∼18 h, a steady and nearly stoichiometric evolution of H_2 and O_2 gases can be observed. No apparent degradation in the photocatalytic activity was observed after 18 h. Repeated experiments yield similar results to those shown in Figure 5b. It is also noted that the pH (∼7.0) of the reactant solution (pure water) was virtually invariant after the reaction.

Additionally, the turnover number (defined as the number of reacted electrons over the number of atoms in a photocatalyst) exceeded 6 after ∼18 h of reaction time. Moreover, the turnover number of our GaN nanowires per unit time is significantly higher than the commonly reported values for powder samples (see Figures S4 and S5 in Supporting Information). These results further confirm that the evolution of H_2 and O_2 gases results from a photocatalytic reaction; i.e., our GaN nanowires are chemically stable in the whole reaction process. Preliminary measurements also show an apparent quantum yield of ∼0.5%. However, the real quantum yield is expected to be significantly higher and can be further improved by optimizing the nanowire surface density, size, and doping concentration, as well as the H_2 evolution sites on the lateral surfaces of the nanowires. Moreover, through the use of tunable band gap epitaxial InGaN nanowires, high-efficiency overall water splitting, and H_2 production under direct solar irradiation is anticipated and currently under investigation.

In summary, we have demonstrated that nonpolar GaN surfaces possess the capacity for both H_2 and O_2 evolution. With the incorporation of photodeposited Rh/Cr_2O_3 core−shell structures as cocatalysts, photocatalytic pure water splitting is

dx.doi.org/10.1021/nl2006802 |*Nano Lett.* 2011, 11, 2353–2357

achieved, for the first time, on III−nitride nanowires. This work establishes the use of III−nitride nanowire heterostructures as viable photocatalysts for achieving stable and efficient water splitting and H_2 generation directly from solar irradiation. Moreover, the realization of wafer-level photocatalytic water splitting (compared to conventional powder based approaches) promises low cost, high performance, and compact hydrogen production systems that were not previously possible.

■ ASSOCIATED CONTENT

Supporting Information. Photodeposition of Rh/Cr_2O_3 core−shell nanostructures, evaluation of photocatalytic water splitting, photoluminescence spectrum of GaN nanowires, SEM images of GaN films and GaN powders, and photocatalytic activities of GaN nanowire, film, and powder samples for H_2 and O_2 evolution. This material is available free of charge via the Internet at http://pubs.acs.org.

■ AUTHOR INFORMATION

Corresponding Author

*E-mail: zetian.mi@mcgill.ca.

■ ACKNOWLEDGMENT

This work was supported by the Natural Sciences and Engineering Research Council of Canada (NSERC) and Defence Research & Development Canada. Part of the work was performed in the Microfabrication Facility at McGill University. Electron microscopy images and analysis with the Titan 80-300 Cubed was carried out at the Canadian Centre for Electron Microscopy, a National facility supported by NSERC and McMaster University. K.H.B. acknowledges partial support by the U.S. DOE (Grant No. DE-FG02-05ER46209, the Division of Materials Sciences and Engineering, Office of Basic Energy Sciences).

■ REFERENCES

(1) Zou, Z. G.; Ye, J. H.; Sayama, K.; Arakawa, H. *Nature* **2001**, *414*, 625.

(2) Maeda, K.; Teramura, K.; Lu, D. L.; Takata, T.; Saito, N.; Inoue, Y.; Domen, K. *Nature* **2006**, *440*, 295.

(3) Fujishima, A.; Honda, K. *Nature* **1972**, *238*, 37.

(4) Kato, H.; Asakura, K.; Kudo, A. *J. Am. Chem. Soc.* **2003**, *125*, 3082.

(5) Domen, K.; Kondo, J. N.; Hara, M.; Takata, T. *Bull. Chem. Soc. Jpn.* **2000**, *73*, 1307.

(6) Kadowaki, H.; Sato, J.; Kobayashi, H.; Saito, N.; Nishiyama, H.; Simodaira, Y.; Inoue, Y. *J. Phys. Chem. B* **2005**, *109*, 22995.

(7) Maeda, K.; Xiong, A.; Yoshinaga, T.; Ikeda, T.; Sakamoto, N.; Hisatomi, T.; Takashima, M.; Lu, D.; Kanehara, M.; Setoyama, T.; Teranishi, T.; Domen, K. *Angew. Chem., Int. Ed.* **2010**, *49*, 4096.

(8) Luo, W. J.; Liu, B.; Li, Z. S.; Xie, Z. L.; Chen, D. J.; Zou, Z. G.; Zhang, R. *Appl. Phys. Lett.* **2008**, *92*, 262110.

(9) Aryal, K.; Pantha, B. N.; Li, J.; Lin, J. Y.; Jiang, H. X. *Appl. Phys. Lett.* **2010**, *96*, 052110.

(10) Jung, H. S.; Hong, Y. J.; Li, Y.; Cho, J.; Kim, Y. J.; Yi, G. C. *ACS Nano* **2008**, *2*, 637.

(11) Chen, P. T.; Sun, C. L.; Hayashi, M. *J. Phys. Chem. C* **2010**, *114*, 18228.

(12) Shen, X. A.; Small, Y. A.; Wang, J.; Allen, P. B.; Fernandez-Serra, M. V.; Hybertsen, M. S.; Muckerman, J. T. *J. Phys. Chem. C* **2010**, *114*, 13695.

(13) Yang, X. Y.; Wolcott, A.; Wang, G. M.; Sobo, A.; Fitzmorris, R. C.; Qian, F.; Zhang, J. Z.; Li, Y. *Nano Lett.* **2009**, *9*, 2331.

(14) Wang, G. M.; Yang, X. Y.; Qian, F.; Zhang, J. Z.; Li, Y. *Nano Lett.* **2010**, *10*, 1088.

(15) Ahn, K. S.; Shet, S.; Deutsch, T.; Jiang, C. S.; Yan, Y. F.; Al-Jassim, M.; Turner, J. *J. Power Sources* **2008**, *176*, 387.

(16) Wu, N. Q.; Wang, J.; Tafen, D.; Wang, H.; Zheng, J. G.; Lewis, J. P.; Liu, X. G.; Leonard, S. S.; Manivannan, A. *J. Am. Chem. Soc.* **2010**, *132*, 6679.

(17) Hochbaum, A. I.; Yang, P. D. *Chem. Rev.* **2010**, *110*, 527.

(18) Wolcott, A.; Smith, W. A.; Kuykendall, T. R.; Zhao, Y. P.; Zhang, J. Z. *Small* **2009**, *5*, 104.

(19) Ding, Q. P.; Yuan, Y. P.; Xiong, X.; Li, R. P.; Huang, H. B.; Li, Z. S.; Yu, T.; Zou, Z. G.; Yang, S. G. *J. Phys. Chem. C* **2008**, *112*, 18846.

(20) Li, Y.; Zhang, J. Z. *Laser Photonics Rev.* **2010**, *4*, 517.

(21) Maeda, K.; Teramura, K.; Saito, N.; Inoue, Y.; Domen, K. *Bull. Chem. Soc. Jpn.* **2007**, *80*, 1004.

(22) Bertness, K.; Roshko, A.; Sanford, N.; Barker, J.; Davydov, A. *J. Cryst. Growth* **2006**, *287*, 522.

(23) Seelmann-Eggebert, M.; Weyher, J. L.; Obloh, H.; Zimmermann, H.; Rar, A.; Porowski, S. *Appl. Phys. Lett.* **1997**, *71*, 2635.

(24) Kudo, A.; Miseki, Y. *Chem. Soc. Rev.* **2009**, *38*, 253.

(25) Nozik, A. J.; Memming, R. *J. Phys. Chem.* **1996**, *100*, 13061.

(26) Van de Walle, C. G.; Segev, D. *J. Appl. Phys.* **2007**, *101*, 081704.

(27) Bertelli, M.; Loptien, P.; Wenderoth, M.; Rizzi, A.; Ulbrich, R. G.; Righi, M. C.; Ferretti, A.; Martin-Samos, L.; Bertoni, C. M.; Catellani, A. *Phys. Rev. B* **2009**, *80*, 115324.

(28) Hata, H.; Kobayashi, Y.; Bojan, V.; Youngblood, W. J.; Mallouk, T. E. *Nano Lett.* **2008**, *8*, 794.

(29) Ma, R. Z.; Kobayashi, Y.; Youngblood, W. J.; Mallouk, T. E. *J. Mater. Chem.* **2008**, *18*, 5982.

(30) Maeda, K.; Teramura, K.; Lu, D. L.; Takata, T.; Saito, N.; Inoue, Y.; Domen, K. *J. Phys. Chem. B* **2006**, *110*, 13753.

(31) Maeda, K.; Sakamoto, N.; Ikeda, T.; Ohtsuka, H.; Xiong, A. K.; Lu, D. L.; Kanehara, M.; Teranishi, T.; Domen, K. *Chem.—Eur. J.* **2010**, *16*, 7750.

(32) Yoshida, M.; Takanabe, K.; Maeda, K.; Ishikawa, A.; Kubota, J.; Sakata, Y.; Ikezawa, Y.; Domen, K. *J. Phys. Chem. C* **2009**, *113*, 10151.